Review

Microfabricated Ultramicroelectrode Arrays: Developments, Advances, and Applications in Environmental Analysis

Rosemary Feeney and *Samuel P. Kounaves**

Department of Chemistry, Tufts University, Medford, MA 02155, USA

Received: December 9, 1999
Final version: January 11, 2000

Abstract
The wider availability of microlithographic techniques for the fabrication of electrochemical devices has led to a significant increase in the development of microfabricated arrays of microelectrodes and their use in a wide variety of analytical problems. The major microfabrication steps and the capabilities and limitations of this microsensor technology are reviewed in this article. Several examples are summarized to illustrate the breadth of work with silicon-based microelectrode arrays, with special emphasis on their use for environmental analysis in a range of diverse settings including remote electroanalysis on Mars.

Keywords: Microfabrication, Ultramicroelectrode, Arrays, Electroanalysis, Sensors

1. Introduction

In recent years, the electroanalytical use of microlithographically fabricated arrays of microelectrodes has dramatically increased. Photolithographic techniques, widely used in the microelectronics industry, have been utilized to construct electromechanical sensors since the late 1970's [1]. This technology can effectively pattern and build thin film electrode materials such as iridium, platinum, gold, and carbon on silicon wafers, with well-defined and reproducible geometries of micron dimensions. Modern micromachining technologies have enabled the mass production of individual chip-based sensors that possess identical physical and chemical performance characteristics, an important criteria for widespread commercialization and use of any sensor technology. Silicon has been the material of choice and has been widely used to fabricate complex integrated circuits and physical sensors due to inexpensive manufacturing cost in high volumes [2–4].

One important impetus for development of electrochemical sensors lies with the increasing emphasis on environmental issues, such as waste reduction, contamination of natural water system, and improving industrial operations [5]. More specifically, the pragmatic analytical requirements imposed by the remediation and monitoring of a growing number of contaminated sites and the huge labor and analytical costs can be substantially reduced by rapid field screening tools. Many of these sensors are based on established electroanalytical techniques such as stripping voltammetry and have gained new applicability due to their compact size, high sensitivity, and low cost [6] (Table 1). Arrays of ultramicroelectrodes (UMEAs) have been demonstrated as an especially effective and viable analytical screening tool for heavy metals in natural waters [6–13].

However, both fabrication and analytical problems, many of which are still not well understood, have restrained the widespread use of microfabricated UME arrays. These have included: deviations from theory due to spacing of the individual UMEs, variability in mercury plating efficiency, apparent inability of different microfabrication facilities in producing identical thin films such as Ir, the deposition of pin-hole free insulation layers, layer adhesion, and the lack of data in the use and characterization of such devices in aqueous environments. Thus, with each alteration in design or of a microfabrication step, a new sensor may exhibit a different electrochemical behavior and analytical response. Unless better understood, such factors may present uncertainties that limit sensor reliability and prevent such technology from being fully exploited as analytical devices.

This review focuses on developments during the past decade in several areas including, microfabrication processes, characterization techniques, basic studies, and applications for the measurement of inorganic metal ions in a variety of natural environments, including recent implementation for remote in situ analysis of the soil on Mars.

2. Thin-Film Microfabrication Technology

In general, a standard silicon wafer, with a thermally grown oxide layer, is the base on which microelectrode structures are built using a series of photolithographic masks and deposition techniques. A seed layer, approximately 100 Å thick, of either Cr

Table 1. Recent patents for the microfabrication of UME array devices.

Assembly	*Patent number (year)*	*Designation*	*Authors*
Ir(Hg) UMEA	US 5378343 (1995)	USA	S. P Kounaves et al.
Pt, Au, graphite UMEAs	DE 94-4422049 (1996)	Germany	K. Cammann et al.
Metal or metal alloys, array of UMEs	WO 97-CA236 (1997)	International	G. Y. Champagne et al.
Iridium UMEA/agarose	EP 780684 (1997)	European	J. Buffle et al.

  1040-0397/00/0905–0677 $17.50+.50/0

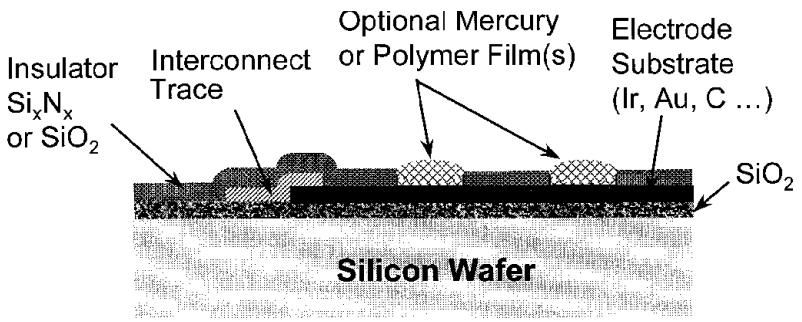

Fig. 1. Cross-sectional diagram of a typical microfabricated UME array device. Arrays are typically fabricated on a 10 cm silicon wafers and diced into individual sensor chips. (Not to scale.)

or Ti is usually deposited prior to depositing the thicker electrode metal layer in order to improve adhesion. Thin films of materials such as iridium, gold, platinum, and carbon can be deposited in a number of ways, including chemical vapor deposition (CVD), electron beam evaporation, or magnetron sputtering of a target. A photocurable organic resist is then deposited on top of the electrode material by spin coating. The resist is patterned using UV radiation through a photomask with desired design pattern. Depending on the features required, the resist can be made soluble or insoluble (i.e., positive or negative) using radiation in a developing solution.

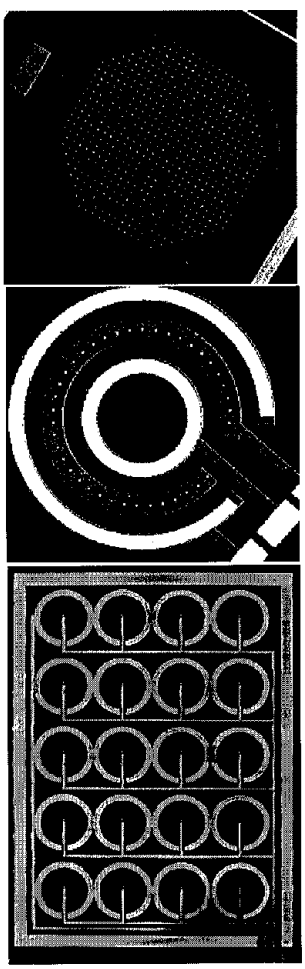

Fig. 2. SEM images of typical microfabricated array designs. Top) A "honeycomb" pattern of 564 10-μm diameter UMEs. Center) A "ring" design with 40 10-μm diameter UMEs. Outer and inner rings are on-chip counter and reference electrodes, respectively. Bottom) A "bicycle" design of 20 10-μm diameter UMEs, each surrounded by a ring couter/reference electrode.

Two strategies can be implemented to pattern the requisite electrode features. The first involves a "lift-off procedure" and is a prerequisite for fabrication of microscale iridium components [14]. In this case, the resist is patterned over the thin metal film and developed as above. Next, the metal is deposited on top of the resist where it adheres well only to the resist-free regions. By dissolving the underlying resist in an appropriate solvent, the unwanted metal falls away. In the second approach, the previously patterned resist protects the underlying metal layer during subsequent etching processes. Wet-etching involves oxidation-reduction reactions for metals and acid-base reactions for inorganic oxides [15]. Dry-etch methods encompass sputtering, plasma, or reactive ion etching. The etching process is commonly used, but is still poorly understood. Finally, the resist can be stripped in an appropriate solvent, typically a hot acid bath or by exposure to oxygen plasma. After the electrode structures have been built, an insulating layer is deposited and patterned across the wafer. Insulating layers commonly used are Si_3N_4, SiO_2, SiC, or polyimide and are applied in various thicknesses ranging from 1500 Å to 5000 Å. These layers are generally deposited by plasma enhanced chemical vapor deposition (PECVD) and reactive ion etch (RIE) can be used to open the UMEs and bond pads. The insulating layer needs to maintain good adhesion to the metal. Sometimes an additional layer of Cr, or Ti is used to insure the structural integrity of the UME wells and to keep solution from reaching the interconnect traces. Figures 1 and 2 illustrate a typical microfabricated UME array device.

3. Theory

3.1. Spacing of the UMEs

There are several articles in the literature which discuss the theoretical analytical response of UMEAs and the parameters that affect it [16–19]. Morf and de Rooij [17] presented theoretical calculations for the current output of arrays of different packing densities using steady-state and chronoamperometric responses. Densely packed arrays were considered to have an interelectrode distance of 2 times the radius, whereas the interelectrode distance for loosely paced arrays was $d \gg 2r_o$. In the analysis, an array of loosely packed electrodes yielded a near ideal multiple response of a single ultramicroelectrode and the closely packed array more closely resembled the behavior from a macroelectrode of a

similar surface area. It was poignantly demonstrated that only when the interelectrode distance between individual UMEs is sufficiently large are the benefits of using an array achieved. In another article, Morf [16] presented a theoretical approach to the steady-state behavior of multiple microelectrode arrays consisting of spherical, hemispherical, disk-shaped or hemicylinderical electrodes. Theories were developed with restriction on the mass transport between bulk solution and electrode to a stagnant diffusional layer (δ_{ss}) of average thickness. At short analysis times, with an array of N microelectrodes, the current response was dominated by nonlinear diffusion to the individual microelectrodes. At longer times however, the overlap of diffusion layers occurred and diffusion became linear to the entire surface of the array [20]. Morf concluded that the average interelectrode distance between electrodes is the most critical parameter to optimize array output response regardless of the geometry. He also noted that as the distance between electrodes increases, the current densities decrease. Only at the lowest current densities was an optimum current response obtained which corresponded well to theory.

The sensitivity of UMEAs to convection has also been considered. The reduction of the convection-dependent contribution to $<10\,\%$ of the signal for an array with $2r_o = 1\,\mu m$ and $\delta = 150\,\mu m$, requires that the interelectrode distance be greater than $50\,\mu m$ [18]. With the total current of the array also reduced to the same percentage relative to the output of a macroelectrode, an ideal convection-independent response behavior can only be achieved for an array with extremely low current efficiencies. Experimental work by Belmont et al. [7] suggested that separation distances should be 10 times the diameter of the electrode. Using this interelectrode distance, the theoretical current response compared well with the experimental values for times $<1000\,s$, when taking into account the slight recess of the electrode surface and the hexagonal packing of the UMEs.

Weber [19] formulated simple models for chronoamperometry in quiescent and nonquiescent (noisy) solutions, incorporating radial diffusion and using a 2 dimensional array of electrodes. It was determined that the electrochemically active area depends on noise power and resistance, background current, electrode capacitance and current density. The noise was found to be proportional to the electrode area and capacitance in amperometry and voltammetry. For densely packed arrays with small UMEs, significant improvement in the signal to noise ratio was observed, however, ohmic interactions were found to increase with the number of neighboring electrodes and remain significant if the separation distance is <10 times the radii [21]. Thus, there appear to be several reasons for keeping the UME separation $d \gg r$.

3.2. Chemometric Treatment of Data

Chemometric analysis is commonly used with many sensors, yet application to voltammetrically obtained data has been limited. A good example of its use with an array of macroelectrodes is that reported by Winquist et al. [22] where they demonstrated the concept of using multivariate signal processing to extract voltammetric information from milk samples using various large electrodes in an assembly. Models for predictions were made and both artificial neural networks (ANN) and principal component analysis (PCA) were used. After training, the models satisfactorily predicted the course of bacterial growth in milk samples. Recently, several studies have shown the utility of applying such techniques to arrays of voltammetric electrodes [23–25].

Glass et al. [24] described an early use of a multielement microelectrode array with which statistical methods were used to maximize the information content from the voltammetric measurements. Their goal was to optimize sensor design and experimental protocol using a matrix of electrode materials (Pt, Au, V, Ir, and C) and to ultimately develop sensors capable of detection and identification of a variety of compounds. The responses from this array could then be evaluated using a probabilistic information model. The basic theory is based in principle on the concept of entropy, and expresses increased information in terms of decreased uncertainty and uses weighted averages of even probabilities to quantify information content. It was found that an enhancement of 25 % in information over a single electrode material was achieved and demonstrated a method to rapidly screen signals from several electrode materials for optimization of an array.

Similarly, a combinatorial approach for optimizing the information obtained from electrodes modified in a variety of ways was investigated by Sullivan et al. [25]. This approach minimized the inefficiencies in screening various compositional variables of complex systems and comparing the performance of different electrode materials using electrochemical methods due to voluminous amount of experimental variables. The group successfully demonstrated this approach for automated screening of electrochemical activity of modified gold surfaces. In previous studies, fluorescence measurements had been used in conjunction with electrode reactions that produce pH changes. In this way, no direct electrochemical measurement would be made, resulting in the inability of distinguishing small differences in electrode activity. The microfabricated device studied consisted of 64 individually addressable gold microelectrodes and were either unmodified or modified with several thiol compounds. Cyclic voltammetry was used to generate the signal. The pattern of alkanethiols used across the array was depicted in a matrix, which showed good correlation between the electrochemical signal and length of thiol chain. These preliminary findings demonstrated the efficacy of this approach to rapid screening for electrode material and systems. In this way, automated chemical measurements, distinguished successfully, the small changes in activity due to the modification of the electrode surface with hexanethiol directly and did not require continuous operator input.

Wehrens et al. [23] demonstrated the calibration of an array containing individually modified surfaces of Au, Rh, Ir, and Pt microelectrodes. In this study, the concentrations of variously substituted benzene compounds were analyzed for by using linear scan voltammetry. In addition, two calibration methods were utilized, principal component regression and an artificial neural network. Even though both techniques are well known, they have only been sparingly used with voltammetric sensors. These advanced calibration methods are very useful over linear calibration methods due to the nonlinear nature of the data produced by sorption processes. Various data representations were also tested and success of the method was extremely dependent on those representations. Comparisons were made between the two methods, with the neural networks yielding better results.

4. Characterization

Full characterization and optimization of these devices requires a multidisciplinary approach. Sensitive surface techni-

ques combined with basic electrochemical studies are necessary to understand the complex processes occurring at the array surface. Thus, the widespread application of microfabricated arrays in routine analyses will only come about through concerted interdisciplinary efforts by electrochemists, microfab engineers, and surface analysis specialists. Several articles have been highlighted to illustrate the various methods employed in characterizing and optimizing the analytical capabilities of the UMEAs.

4.1. Surface Analyses

Wittkampf et al. [26] presented surface analyses of UMEAs by TOF-MS, SIMS, SEM, and STM and demonstrated the utility of these techniques in assessing the quality of UMEAs. With the TOF-SIM, they found trace silver from the on-chip Ag/AgCl reference and aluminum due to inadequate removal of the adhesion layer. However, no organic contaminants were found. Field emission SEM and STM were used to obtain images of the platinum surface. The platinum thin film was found to be polycrystalline with grain sizes in the 100–700 nm range. The effective surface area in comparison to geometric area was expected to be larger due to surface features seen under high magnification. The increased surface area was attributed to the roughness caused by the nanocrystallites, the large grain sizes and boundaries, and the cavity between the platinum microelectrode and the insulating layers [26]. Although this may seem to be an extreme case, it clearly demonstrates the necessity of using sensitive surface techniques to find imperfections which can cause irreproducibility in the electrochemical behavior of the array.

4.2. Fabrication Shortcomings

A wide variety of common problems that affect silicon-based micromachined devices when used in electrolyte solutions was documented and explained by Schmitt et al. [27]. Problems were generally attributed to insufficient barrier properties and poor corrosion resistance of common passivation layers. SEM images, layer resistance measurements, and detection of leak currents, helped to identify the failure mechanisms caused by mechanical stresses, film defects (pinholes and particle inclusions), sorption processes, corrosion, swelling and diffusion processes. The group concluded that duplex layers of SiO_2/Si_3N_4 and triplex layers of oxide/nitride/oxide with optimized nitride PECVD yielded the best barrier protection. In another study by Nolan and Kounaves [28] it was shown that an array fabricated with aluminum traces failed in solutions containing >0.1 M Cl^-. The failure in this case was attributed to penetration of Cl^- through the insulating layer and its subsequent reaction with the Al interconnect traces. It was recommended that locating the traces inside the thermal SiO_2 layer and substituting gold for aluminum can prevent such failure of a microfabricated devices [27, 28].

4.3. Mercury Plating Efficiency on UMEAs

In many analytical procedures, Pt and Ir arrays are used in conjunction with a film of mercury on their surface. In such cases, the reduction (Q_{red}) and oxidation (Q_{ox}) charges are monitored during the deposition and stripping cycles of mercury and the results can be used as a predictor of array lifetime. Nolan and Kounaves[29] monitored changes to an iridium array (20 10-μm diameter UMEs with $d > 90$ μm) under such cycling both electrochemically and with an AFM. Prior to use, AFM images showed an atomically flat thin-film Ir surface with no obvious deformities. Repetitive electrochemical use of Ir roughens the surface to some extent. In theory, no matter how many times mercury is deposited and stripped, the efficiency (Q_{ox}/Q_{red}) should be 100 %. Experimentally though, efficiencies are typically much lower. For example, the Ir UMEA has been found to give efficiencies ranging from a high of 75 % to a low of 40 %. It has been demonstrated that the low efficiencies can be attributed to calomel formation when Cl^- ions are present in the plating solution by partially covering the surfaces of the mercury, in effect decreasing the amount of mercury which can be reoxidized off the electrode [29]. However, even with careful control, efficiencies of 100 % are not attainable for several reasons, namely that all the liquid mercury is not completely stripped from the Ir, mercury can be chemically oxidized by trace amounts of dissolved O_2 in solution, and capacitive currents can substantially contribute to the deposition charge (Q_{red}).

Belmont et al. [7] also investigated the reliability of mercury drop formation on iridium arrays (100 5-μm diameter UMEs with $d > 150$ μm). After ten consecutive deposition and stripping cycles, their percent efficiency varied between 39 and 81 %, in agreement with the work by Nolan and Kounaves [29]. Reproducibility, assessed using Pb^{2+} and Cd^{2+} at nM concentrations, was excellent with the stripping signal varying by only 4 %. Linear calibrations were performed on 3 separate arrays in a solution containing Pb^{2+} and Cd^{2+}. The resulting regression coefficients were $\geqslant 0.998$ for both metals in the range of 1 to 10 nM. In order to accurately compare the overall average peak current intensity they normalized peak currents (due to different mercury drop sizes). Thus, for the 3 arrays, the normalized peak current for lead was 2.3 nA/nM μm with a standard deviation of 14 % and 1.8 nA/nM μm and a deviation of 25 %.

5. Applications

Heavy metal contamination has gained increasing attention due to its significant and detrimental impact on the environment. A major thrust for research and development of microfabricated arrays has come from the need for rapid on site environmental analysis. These sensors are field deployable, relatively inexpensive, can be modified chemically, or coated with a polymer or mercury film, to provide a selective response. Capable of being used with several electroanalytical methods, microfabricated arrays provide the basis for sensitive and rapid analysis in a variety of settings ranging from neuroscience applications, to highly corrosive media, to complex environmental samples [8, 9, 30, 31]. We have limited this review to the use of microfabricated arrays for determination of heavy metals in environmental samples. Several articles will be highlighted (Table 2) to serve as a representation of the large body of literature which now exists on this topic.

5.1. Heavy Metals

With the need for real-time high quality data being so critical in the assessment of groundwater contaminated by heavy metals at purported hazardous waste sites, the focus of many research

Table 2. Selected examples of the breadth of work performed with silicon-based microfabricated arrays.

Arrays	*Analytes*	*Media*	*Method*	*References*
Au, Pt(Hg)[a]	Pb^{2+}, Cd^{2+}, Cu^{2+}, Hg^{2+}	Acetate buffer	SWASV	[35, 36]
Ir(Hg)[b]	Ni^{2+}	Ammonia buffer	SWCSV, PSA	[38]
Pt(Hg)[c]	Pb^{2+}, Cu^{2+}	Bay water	DPASV	[12]
Ir(Hg)/agarose[d]	Pb^{2+}, Cd^{2+} Mn^{2+}, Zn^{2+}	River and Lake water	SWASV	[7, 8]
Ir(Hg)[e]	Pb^{2+}, Cd^{2+}	KNO_3	SWASV	[37]
Ir(Hg), Ir[b,f]	Pb^{2+}, Zn^{2+}, Cd^{2+}, Cu^{2+}, Se^{4+}, As^{3+}, Hg^{2+}	Ground water, drinking water, Synthetic solutions	SWASV	[9–11, 33, 34]
Ir(Hg)	Trace metals	HF	SWASV	[30]
Au[g]	$Ru(NH_3)_6^{3+}$	KNO_3	CV	[39, 40]
Pt[h,i]	H_2O_2, urea, NH_4Cl	Swimming pool water, buffer solution	CV, amperometry	[44, 50]

[a] 26×26 array of 3-μm diameter UMEs. Interelectrode distance is 30 μm.
[b] 564 10-μm diameter UMEs in a honeycomb pattern. Interelectrode distance is 56 μm.
[c] 50-μm diameter UMEs.
[d] 10×10 array of 5-μm diameter UMEs. Interelectrode distance is 150 μm.
[e] 30×30 array of 5-μm diameter UMEs. Interelectrode distance is 180 μm.
[f] 20 10-μm diameter UMEs in a ring design. Interelectrode distance is <100 μm.
[g] 15 4-μm UMEs and 2 50-μm UMEs.
[h] 3×3 array of 10-μm diameter UMEs.
[i] 10×10 array of 2-μm diameter UMEs. Interelectrode distance is 20 μm.

groups, including ours, has been on the development of microfabricated arrays as devices capable of performing in situ and/or on-site analysis. We have developed and demonstrated a field portable electrochemically based device for real time measurements of Pb^{2+}, Cu^{2+}, Cd^{2+}, Zn^{2+} in surface or ground water at ppt to ppb level [9]. In conjunction with SWASV, both labile and total (pH<2) forms of Zn^{2+}, Cd^{2+}, Pb^{2+}, Cu^{2+} were measured at ppb levels. Results indicated that in situ measurements of labile metal species are feasible and provided a rough estimate of metal concentrations. Comparisons were made to EPA method 200.7 with agreement between data to within an order of magnitude. The system consisted of a laptop computer attached to a probe containing the potentiostat and an array of twenty 10 μm diameter UMEs seperated by 100 μm. The IC-based potentiostat and microcontroller, powered by four 9-volt batteries, was custom built by CIS at Stanford University. The Ir UMEA and external reference electrode were mounted in a PVC connector and covered with an outer PVC tube with holes to allow water flow. This lower unit of the probe was connected to a second piece of PVC tubing, which encapsulated the potentiostat and controller. A 33 m shielded cable feed through to the electronics. Recently, modifications to this sensor probe have been made. In a novel combination, the Ir UMEA was incorporated in a 15 cm long tube containing a Pt counter and reference electrode with a gel filling solution [32]. These design modifications made the probe more compact and rugged.

This same approach has also been recently extended to the detection of Hg^{2+}, As^{3+}, and Se^{4+} at the ppb level in natural water samples [10, 33, 34]. For As^{3+} and Se^{4+}, arrays were fabricated with gold UMEs in a honeycomb pattern of 564 10-μm diameter disks ($d = 56$ μm), providing significant signal amplification. Good performance was shown with a signal reproducibility of 4.5 % for Se^{4+} and 2.5 % for As^{3+} over 10 consecutive runs of a standard solution. The reported limits of detection were 0.42 ppb Se^{4+} ($t_d = 200$ s) and 0.05 ppb As^{3+} ($t_d = 300$ s). Since the theory for SWASV has only been solved for a thin mercury film, the influences of SW frequency, pulse amplitude and deposition potential on the As^{3+} and Se^{4+} stripping peaks were investigated. Interestingly, it was determined that similar phenomena occur at bare metal electrodes. For a thin film, it is predicted that Δi_p is proportional to f, thus an increase in SW frequency should result in a linear increase in stripping peak height. Results were suprisingly similar to that of the thin mercury film case [10]. To characterize the deposition of As^{3+} or Se^{4+} on the Au-UMEA, a plot of the peak stripping current vs. deposition potential was made. Experimental data collected by applying cathodic deposition potentials. Theoretical curves were calculated for each metal using the relationship $E_{dep} = E_{1/2} - (0.0592/n)\ \log\ (i/i_d - i)$. Linearity calibration plots were obtained for both metals with the regression coefficient $\geqslant 0.991$ for 10–100 and 0–400 ppb.

Most recently it has been demonstrated that Ir itself can be directly used as an electrode material for rapid analysis of Cu^{2+} or Hg^{2+} in natural water samples [34]. Even though bare indium suffers from a small potential window between the hydrogen reduction reaction and indium oxidation, metals such as Cu^{2+} or Hg^{2+}, whose redox potential falls within these limits, can be detected in conjunction with an appropriate choice of supporting electrolyte. The Ir-UMEA with 564 (10 μm diameter UMEs with $d = 56$ μm) showed remarkable reproducibility in the signals for either metal and had the ability to detect 100 parts-per-trillion Hg^{2+}. Interference studies using Pb^{2+}, Cd^{2+}, and Zn^{2+} were tested and showed little or no effect on the signal. Only Cu^{2+} or Hg^{2+} perturbed the other stripping signal. Drinking water samples were separately analyzed for Cu^{2+} or Hg^{2+} and values were compared to atomic absorption spectrometry, as well as to classical electrochemical analysis with Hg on GCE with excellent correlation. This Ir UME array demonstrated lower standard deviation of the stripping signals with respect to copper.

Uhlig et al. [35, 36] fabricated arrays of Pt, Ir and Au for determination of Cu^{2+} Pb^{2+}, Cd^{2+} and Hg^{2+}. Mercury depositions were investigated on a 26×26 array of 3 μm diameter Pt UMEs separated by 30 μm. They found the mercury film formed on the Pt UMEA to be homogeneous as opposed to the individual droplets formed on a Pt microelectrode. They reasoned that the well created on the chip by using an insulating layer thickness of 500 nm is sufficient to prevent the mercury droplets from spreading out on the Pt surface, resulting in the rapid overlapping of single droplets and film formation. Reproducibility of subsequent mercury film formation was tested by performing

10 SWASV runs of a solution containing Cd^{2+}, Pb^{2+}, Cu^{2+}. Prior to a subsequent analysis, the mercury was stripped and a new film plated. After the 5th analysis, the deviation was still within a 5 % error range and a linear calibration plot with $r^2 = 0.99$ for all metals and concentrations between 1 and 9 ppb. Increased surface roughness of the Pt was observed, and was attributed to formation of an amalgam layer and partial oxidation of Pt. This did not seem to effect the analytical results over the short term. Their reported limits of detection were 100, 300, 500 ng/L at a t_{dep} of 300 s for Pb^{2+}, Cd^{2+} and Cu^{2+}, respectively. A AuUMEA was used for the trace determination of mercury. A linear calibration plot was obtained in HCl with mercury concentrations between 1 and 4 ppb, $r^2 = 0.98$, and with $LOD = 1$ µg/L for $t_{dep} = 1000$ s. Using 50 and 100 µg/L Hg^{2+} solutions, repetitive analysis was also investigated and gave a low RSD of 10 %.

A gel coated mercury Ir array was first used to measure in situ trace metals, Cd^{2+} Pb^{2+}, and Mn^{2+} in lake water by Belmont et al. [8]. The array was comprised of a 10×10 array of 5 µm Ir disk electrodes spaced 150 µm apart. The UMEA was protected by an inert hydrophilic agarose gel. The gel was also used as a dialysis membrane, allowing diffusion of metal ions and small complexes, while hindering colloids and macromolecules, to the surface of the array. The article presents the optimum conditions and characteristics of the gel coated array while monitoring voltammetric signals under convection, temperature, and pressure control. Diffusion profiles of ferricyanide were studied and coefficients were found to be independent of gel thickness from 275 to 600 µm. No retention of the redox complex was observed. Good correlations to theory were observed. Diffusion of Pb^{2+} and Cd^{2+} through a 600 µm gel was measured by SWASV. Coefficients were found to be $(4.2 \pm 0.2) \times 10^{-10}$ m^2/s and $(3.5 \pm 0.2) \times 10^{-10}$ m^2/s for Pb^{2+} and Cd^{2+}, respectively and were independent of gel thicknesses. The authors also studied the influence of convection on these gel coated Ir UMEAs. The current response for microelectrodes should, in theory, not be influenced by convection. However in practice there is a noticeable effect for electrodes >1 µm. Comparing both coated and uncoated UMEAs, the stripping signal for the uncoated array increased by nearly 50 % compared with the agarose coated array. Diffusion did not seem to be enhanced with stirring and the authors suggest that mass transport occurs relatively unhindered via diffusion through the gel.

To demonstrate the protective property of the agarose, a series of experiments were performed using: lake water, natural water with high organic content, and incubation media of bacteria. The results were also compared to ICP-AES analysis. The gel coated array gave comparative results for metals even in the presence of 137 ppm of TOC and containing large polysaccaritic macromolecules released from indigenous bacteria. The unprotected array, however, gave significantly lower signals due to the fouling of the array in such solutions.

Since this sensor was aimed at eventual in situ measurements, the effect of pressure on gel structure was investigated by studying the diffusion of ferricyanide through the agarose film. Using chronoamperometric measurements, they found no effects of pressure on the gel's structure or while using SWASV at 1 to 600 bars. To evaluate any temperature effects, experimental data consisting of SWASV measurements of the diffusion coefficients of Cd^{2+}, Pb^{2+} and Mn^{2+} in $NaNO_3$ or lake water were correlated with theoretical data using the Stokes-Einstein relationship. The plots of $\ln(i)$ vs. $1/T$ and the corresponding slopes were compared to theoretical slopes calculated for reversible systems. Lead fit very well to the theoretical model based on the Arrhenius equation. Slopes for cadmium and manganese showed deviations compared to data for reversible systems. The authors could not explain the deviation of the Cd^{2+}/Cd^0 system, but suggested the results for Mn^{2+}/Mn^0 could be the product of an irreversible system. These results demonstrated the efficacy of the gel coated Ir UMEA for in situ analysis of heavy metals in natural waters.

Silva et al. [37] also reported on development of Ir UMEAs plated with mercury used in conjunction with a newly developed multiple square wave anodic stripping voltammetry (MSWASV). The array consisted of nine-hundred 5-µm diameter disks spaced 180 µm apart. An amorphous 3000 Å thick layer of SiC:H was used to insulated the array. Radial diffusion to the array was confirmed by cyclic voltammetry using hexaaminеruthenium(III) chloride and scan rates between 5 mV/s and 500 mV/s. These results correlate well with the work of Belmont and Morf [7, 16, 37]. The performance of the array was tested using MSWASV in synthetic solutions of Pb^{2+} and Cd^{2+} ions. Over the concentration range 0.5 to 15 µg/L, the signal for both Cd^{2+} and Pb^{2+} was found to be linear with concentration and preconcentration time. Regression coefficients were 0.991 to 0.998 for both metals. LOD was as low was 0.5 µg/L with relatively good reproducibility (about 15 and 30 %). The stability of the mercury film was tested with Cd^{2+} at 1 µg/L with 10 consecutive measurements over a period of 5 hours and yields a standard deviation of 3.5 %.

Adsorptive stripping measurements of trace nickel have been performed by Wang et al. [38] using an Ir based mercury coated UMEA. For this study a Hg coated Ir array of 564 10 µm diameter UMEs separated by 56 µm was used in the presence of dimethylglyoxime. Stripping potentiometry proved to be more sensitive for nickel determination than SWASV in this application. The iridium UMEA displayed greater stability than a mercury coated glassy carbon electrode, which gave a gradual decrease of its nickel stripping peak. The detection limit of 0.5 mg/L and good precision, with a RSD of 1.7 % for 12 consecutive measurements, supports the use of the metal-chelate adsorptive approach for environmental monitoring and expands the application of iridium based Hg microelectrode arrays.

5.2. Multilayered Microfabricated Devices

Fritsch et al. [39] have built individually addressable submicrometer gold band electrode arrays that are 2 mm long and 10–150 nm in width using multilayered materials. The layering technique used to manufacture this device is a promising way to increase the functionality per unit area of the substrate since additional alternating layers of conductor and insulator may be deposited on the substrate and patterned, resulting in multiple electrodes along the wall of a single microfabricated feature. Using cyclic voltammetry with Ru $(NH_3)_6^{3+}$ and a lateral/edge band electrodes with a 50 nm gold thickness layer, it was demonstrated that the magnitude of the pseudo-steady-state current at the edge band electrode is only 65 % lower than that at the lateral band electrode, even though its area was reduced by 98 %. The magnitude of the current predicted by theory for an edge electrode was 50 % less than the lateral electrode, in good agreement with the experimental results [39].

A second article by Fritsch et al. [40] demonstrated an interesting application of microfabrication technology to create arrays of microcavities on a single substrate. These microcavity analyzers could use samples as small as one picoliter. The microcavities were either 50 or 10 µm in diameter and 8 µm deep. Each well has two individually addressable gold electrodes: a recessed

microdisk and a nanoband array in the wall. Approximately 4 μm of polyimide separates each electrode. A comparison was made to models for radial and linear diffusion of both geometries using hexaaminеruthenium(III) chloride. At a scan rate of 100 mV/s, the measured current for the nanoband and recessed microdisk electrode was, within error, as predicted for a hemicylindrical and hemispherical geometry. At a scan rate of 204 V/s, the current increased for the recessed electrode, but deviated from the prediction based on linear diffusion models. It was suggested that a combination of uncompensated resistance and an overcorrection for the background current was the cause. For the nanoband electrode at a scan rate of 204 V/s the measured current exceed the predicted current. It was suggested, however, that there may be an underestimation of the nanoband electrode area, and the definition of the scan period based on the scan rate, may change the calculated current enough to correlate better with the experimental data. In general, Fritsch et al. [40] has successfully demonstrated the proof-of-concept in which a self-contained microfabricated electrochemical device was used for analysis of pico-sized sample volumes.

5.3. Extraterrestrial Environments

Their small size, reproducibility, and rugged construction, make UMEAs ideal candidates for applications where mass, reliability, and power, are critical factors. A very unique and exciting application of these devices, being researched and developed in the Kounaves labs, is their use as part of an array of electroanalytical sensors in the Mars Environmental Compatibility Assessment (MECA) instrument package scheduled to be flown by the National Aeronautics and Space Administration (NASA) on the next Mars Lander [41, 42]. As part of NASA's Human Exploration and Development of Space enterprise, designed and built at the Jet Propulsion Laboratory, MECA seeks primarily to analyze the Martian environment with respect to potential chemical and physical hazards to future human explorers. In the course of its main mission MECA may also provide information of significant value to the planetary and astrobiology communities in terms of the geochemistry and the potential of Mars to support past or present life.

As part of the analytical goals to determine if there are certain hazards associated with the Martian soil, the MECA package includes a Wet Chemistry Laboratory (WCL). The WCL consists of four cells that will accept a sample of Martian soil, which can then be mixed with a leaching solution to determine a broad range of chemical parameters. Each cell contains an array of both voltammetric and potentiometric electrodes. In addition to ion selective electrodes (ISEs) which will be used for determining a variety of soluble cations and anions (e.g., Ag^+, Ca^{2+}, Li^+, Mg^{2+}, Na^+, NH_4^+, Br^-, Cl^-, ClO_4^-, I^-, K^+, NO_3^-, S^-) the cells also each contain a Au-UMEA (512 10-μm UMEs) for determination of metals which can be electrodeposited and analyzed at the ppb levels via square-wave anodic stripping voltammetry (SWASV). The Au-UMEA, designed at Tufts and fabricated by the IBM Watson Research Laboratory, provides an electrode substrate with the ruggedness and sensitivity required for electroanalysis in such a remote and harsh environment.

Preliminary studies indicated that the traditional mercury film used for ASV would not be feasible. In situ mercury plating was not an option due to the possible poisoning of several of the ISEs by the mercury. On the other hand a preplated Hg-film would most likely not survive the long space voyage and extreme environments. Because of these limiting conditions it was decided to attempt solid-state ASV directly on the Au-UMEA. Calibration experiments have shown that Pb, Cu, Hg, and Cd, can be detected and measured at ppb levels using the AuUMEA. Other metals may be deposited and also produce a stripping peak. Unlike typical laboratory electroanalyses, this analysis represents a "single-shoot" experiment at obtaining analytical data from a totally unknown sample. Thus, during the next couple of years a library of possible responses will be developed using Mars simulant soils doped with possible metals.

5.4. Other Applications

There have been several other interesting applications for microfabricated UME arrays. Glass et al. [12] used arrays to monitor Pb^{2+} and Cu^{2+} in plating waste streams in conjunction with a custom built, compact potentiostat, signal generator, and microcomputer. Carbon microelectrode arrays have also peeked interest in recent years. Screenivas et al. [43] described a process of sputter depositing thin conducting films of carbon with improved adhesion to the silicon substrate. Schwake et al. [44] used a Nafion coated Pt UMEA to monitor for hydrogen peroxide levels in swimming pool water and incorporated an on-chip Ag/AgCl pseudo-reference electrode and Pt counter electrode. Williams et al. [45] described the encapsulation of a disposable thin gold film with on-chip pseudo reference and counter electrodes covered by a polystyrene layer. This demonstrated a new process for encapsulation that uses readily available reagents instead of silicon insulating materials. Dobson et al. [46] reported on the fabrication of a gold UMEA and characterized its response in both aqueous and nonaqueous media. Tarasov et al. [47] used gold UMEAs modified with self-assembled monolayers (SAMs), which contain receptor sites that possess affinity for specific metal ions in the presence of others. Application of various thiol modified UMEAs with SWASV provides a sensitive and selective means to measure heavy metals without a preconcentration step. The electrochemical study of the reductive and oxidative removal process of thiol monolayers was performed using various complexes on the gold UMEA. Gold UMEAs were also used as flow sensors in a thin-layer channel by Fosdick et al. [48]. Experimental responses were compared with the theoretical behavior predicted by simulations. One of the earliest descriptions of voltammetry at gold and Pt UMEAs was reported by Thormann et al. [49]. Meyer et al. [50] reported arrays of individually addressable microelectrodes, which allow for redundant measurements as well as multianalyte sensing, to be used as sensors in micro-total-analysis-systems. They successfully demonstrated the ability to image the distribution of ammonium chloride and urea with arrays modified by analyte-selective membranes. Somps et al. [51] have implemented sensor arrays for simple hand-made miniaturized catheter-shaped configurations. They describe options for electrochemical sensors using a combination of thin and thick film technology with nonsilicon substrates using various techniques in a modular approach to designing an integrated sensor for electrolyte and blood gas monitors.

6. Future Work

Photolithographic methods will become increasingly important for the development of micro-total-analysis-systems (μ-TAS). Devices, such as those developed for analysis of excretion

from single cells or vesicles by C.S. Henry's group [40] are self contained electrochemical systems for use in small volume analysis. Such systems will provide advantages when reagents are limited, very expensive, or when needed to scan for many species at once as part of a handheld monitoring instrument. As another example, a nanotitrator has been recently developed at the Institute of Microtechnology Neuchatel in Switzerland [52]. This device integrates a flow-through channel with an electro-osmotically driven nanopump and was successfully used in argentometric, coulometric and acid-base titrations.

Although the achievements of photolithography in developing a variety of electrochemical sensors have been documented, it is still a planar technique, which limits traditional through-mask electroplating in the fabrication of 2-D microstructures with high aspect ratios. Most recently, Whitesides' group goes beyond photolithography and combines soft lithography and microelectrodeposition to fabricate three-dimensional metallic microstructures [53]. Soft lithography uses an elastomeric element in the pattern-transfer step and electroplating ductile metals onto the structures formed by microcontact printing, gives the rigidity necessary for microstructures to be self-supporting. This type of innovation should lead to the development of fascinating new structures and designs for microanalysis. Also, the increasing use of statistical methods in conjunction with arrays will provide a way of rapidly optimizing the design of multielement arrays for detection of numerous species concurrently.

Looking at the future, the use of voltammetric analysis at microfabricated UME arrays appears to be very promising. Their small size, reproducibility, and rugged construction, makes them ideal candidates for implementing a variety of electroanalytical techniques in a variety of environments, from the laboratory bench on Earth to remote sensing on Mars and other planetary bodies.

7. References

[1] T. Gueshi, K. Tokuda, H. Matsuda, *J. Electroanal. Chem.* **1978**, *89*, 247.
[2] G.T.A. Kovacs,. *Anal. Chem.* **1996**, 407A.
[3] G. Bub, M.J. Schoning, H. Luth, J.W. Schultz, *Electrochim. Acta* **1999**, *44*, 3899.
[4] M.K. Andrews, P.D. Harris, *Electroanalysis* **1998**, *10*, 1112.
[5] B. Fleet, H. Gunasingham, *Talanta* **1992**, *39*, 1449.
[6] M.-L. Tercier, J. Buffle, *Electroanlysis* **1993**, *5*, 187.
[7] C. Belmont, M.-L. Tercier, J. Buffle, G. Fiaccabrino, M. Koudelka-Hep, *Anal. Chim. Acta* **1996**, *329*, 203.
[8] C. Belmont-Hebert, M.L. Tercier, J. Buffle, *Anal. Chem.* **1998**, *70*, 2949.
[9] J. Herdan, R. Feeney, S.P. Kounaves, A.F. Flannery, C.W. Storment, G.T.A. Kovacs, *Env. Sci. Tech.* **1998**, *32*, 131.
[10] R. Feeney, S.P. Kounaves, *Anal. Chem.* **2000**, in press.
[11] S.P. Kounaves, W. Deng, P. Hallock, G.T.A. Kovacs, C.W. Storment, *Anal. Chem.* **1994**, *66*, 418.
[12] R.S. Glass, K.C. Hong, J.C. Estill, R A. Reibold, W.M. Thompson, D.W. O'Brien, D.R. Ciarlo, V.E. Granstaff, *Proc. 79th AESF Annu. Tech. Conf.*, Vol. 1 **1992**, p. 83.
[13] J. Wang, B. Tian, J. Wang, J. Lu, C. Olsen, C. Yarnitzky, K. Olsen, D. Hammerstrom, W Bennett, *Anal. Chim. Acta* **1999**, *385*, 429.
[14] R.L. McCarley, M.G. Sullivan, S.C., Y. Zhang, R.W. Murray, in *Microelectrodes: Theory and Applications*, Vol. 197 (Eds: M.I. Montenegro, M.A. Q., J.L. Daschbach), Kluwer, Dordrecht, The Netherlands, **1991**.
[15] G.C. Fiaccabrino, M. Koudelka-Hep, *Electroanalysis* **1998**, *10*, 217.
[16] W.E. Morf, *Anal. Chim. Acta* **1996**, *330*, 139.
[17] W.E. Morf, N.F. de Rooij, *Sens. Actuators B* **1997**, *44*, 538.
[18] W.E. Morf, N.F. de Rooij, *Sens. Actuators A* **1995**, *51*, 89.
[19] S.G. Weber, *Anal. Chem.* **1989**, *61*, 295.
[20] B.R. Scharifker, in *Microelectrodes: Theory and Applications*, Vol. 197 (Eds: M.I. Montenegro, M.A. Q., J.L. Daschbach) Kluwer, Dordrecht, The Netherlands **1990**.
[21] A. West, *J. Electrochem. Soc.* **1993**, *140*, 134.
[22] F. Winquist, C. Krantz-Rulcker, P. Wide, I. Lundstrom, *Meas. Sci. Technol.* **1998**, *9*, 1937.
[23] R. Wehrens, W.E.v.d. Linden, *Anal. Chim. Acta* **1996**, *334*, 93.
[24] R.S. Glass, S.P. Perone, D.R. Ciarlo, *Anal. Chem.* **1990**, *62*, 1914.
[25] M.G. Sullivan, H. Utomo, P.J. Fagan, M.D. Ward, *Anal. Chem.* **1999**, *71*, 4369.
[26] M. Wittkampf, K.C.M. Amrein, R. Reichelt, *Sens. Actuators B* **1997**, *40*, 79.
[27] G. Schmitt, J.W. Schultze, F. Fassbender, G. Buss, H. Luth, M.J. Schoning, *Electrochim. Acta* **1999**, *44*, 3865.
[28] M.A. Nolan, S.P. Kounaves, *Sens. Actuators B* **1998**, *50*, 117.
[29] M.A. Nolan, S.P. Kounaves, *J. Electroanal. Chem.* **1998**, *453*, 39.
[30] S. Tsai, S. Tan, A.F. Flannery, C.W. Storment, G.T.A. Kovacs, *AIP Conf. Proc.* **1998**, 907.
[31] T.T. Nordhausen, E.M. Maynard, R. Normann, *Brain Res.* **1996**, *726*, 129.
[32] J. Herdan, S.P. Kounaves, X. Wen, S.J. West, *216th ACS Nat. Meet., Book of Abstracts, Boston, Massachusetts, August 23–27* **1998**.
[33] S. H Tan, S.P. Kounaves, *Electroanalysis* **1998**, *10*, 364.
[34] M.A. Nolan, S.P. Kounaves, *Anal. Chem.* **1999**, *71*, 3567.
[35] A. Uhlig, U. Schnakenberg, R. Hintsche, *Electroanalysis* **1997**, *9*, 125.
[36] A. Uhlig, M. Paeschke, U. Schnakenberg, R. Hintsche, H. Hoachim Diederich, F. Scholz, *Sens. Actuators B* **1995**, *24–25*, 899.
[37] P.R.M. Silva, M.A. El Khakani, M. Chaker, G.Y. Champagne, J. Chevalet, L. Gastonguay, R. Lacasse, M. Ladouceur, *Anal. Chim. Acta* **1999**, *385*, 249.
[38] J. Wang, J. Wang, W.K. Adeniyi, S.P. Kounaves, *Electroanalysis* **1999**, *12*, 96.
[39] M.P. Nagale, I. Fritsch, *Anal. Chem.* **1998**, *70*, 2908.
[40] C.S. Henry, I. Fritsch, *J. Electrochem. Soc.* **1999**, *146*, 3367.
[41] T.P. Meloy, J. Marshall, M. Hecht, in *Workshop on Mars 2001: Integrated Science in Preparation for Sample Return and Human Exploration* (Eds: J. Marshal, C. Weitz), LPI Contribution 991, Lunar and Planetary Institute, Houston **1999**, pp. 74–76.
[42] S.M. Grannan, M. Frant, M.H. Hecht, S.P. Kounaves, K. Manatt, T.P. Meloy, W.T. Pike, W. Schubert, S. West, X. Wen, in *Workshop on Mars 2001: Integrated Science in Preparation for Sample Return and Human Exploration* (Eds: J. Marshal, C. Weitz), LPI Contribution 991, Lunar and Planetary Institute, Houston **1999**, pp. 41–42.
[43] G. Screenivas, S. Ang, I. Fritsch, W. Brown, G. Gerhardt, D. Woodward, *Anal. Chem.* **1996**, *68*, 1858.
[44] A. Schwake, Ross, B., K. Cammann, *Sens. Actuators B* **1998**, *B46*, 242.
[45] G. Williams, C. D'Silva, *Sens. Actuators B* **1996**, *30*, 151.
[46] P. Dobson, L. Jiang, P.A. Leigh, Hill, H. A., S. Kaneko, *Adv. Mater. Opt. Electron.* **1992**, *1*, 133.
[47] V.V. Tarasov, S.P. Kounaves, *New Orleans, LA, March 1–5* **1998**, *Pittsburgh Conference*.
[48] L. Fosdick, J. Anderson, T. Baginski, R. Jaeger, *Anal. Chem.* **1986**, *58*, 2750.
[49] W. Thormann, P. Van den Bosch, A.M. Bond, *Anal. Chem* **1985**, *57*, 2764.
[50] H. Meyer, B. Naendorf, M. Wittkampf, B. Grundig, K. Cammann, R. Kakerow, Y. Manoli, W. Mokwa, M. Rospert, *MESA Research Institute, University of Twenty*, Kluwer, The Netherlands **1994**, p. 245.
[51] C.J. Somps.M.J. Madou, J.W. Hines, *SPIE* **1998**, 199.
[52] O.T. Guenat, G.C. Fiaccabrino, W. Morf, E. Werner, M. Koudelka-Hep, N.F. de Rooij, *Chimia* **1999**, *53*, 87.
[53] R.J. Jackman, S.T. Brittain, A. Adams, H. Wu, M.G. Prentiss, S. Whitesides, G.M. Whitesides, *Langmuir* **1999**, *15*, 826.